

Analytical blueprint for 99.999% fidelity X-gates on present superconducting hardware under strong driving

José Diogo Da Costa Jesus,^{1,2} Boxi Li,¹ Yuan Gao,^{3,4} Rami Barends,^{3,4} Francisco Andrés Cárdenas-López,¹ and Felix Motzoi^{1,2}

¹*Institute for Quantum Control (PGI-8), Forschungszentrum Jülich, 52425 Jülich, Germany*

²*Institute for Theoretical Physics, University of Cologne, 50937 Cologne, Germany*^{*}

³*Institute for Functional Quantum System (PGI-13), Forschungszentrum Jülich, 52425 Jülich, Germany*

⁴*Department of Physics, RWTH Aachen University, 52074 Aachen, Germany*

(Dated: December 24, 2025)

Achieving very fast gates that undercut the natural limits set by decoherence requires going into the strong driving limit. Realizing single-qubit control predicted beyond semi-classical, time-dependent modeling has yet to be experimentally realized on superconducting and most other computing platforms. In this regime, the common model of dynamics within a three-level manifold breaks down, and instead, we see new quantum error channels growing abruptly with decreasing time. To identify these error processes we systematically calculate the effect of multi-photon transitions that occur out of the computational space. We then derive analytical formulas to suppress these effects, as well as amplitude and phase errors on the qubit space; we term these R1D for suppressing the $|0\rangle \rightleftharpoons |2\rangle$ transition and R2D when also suppressing $|1\rangle \rightleftharpoons |3\rangle$ leakage. We also answer long-standing questions about the optimal values of the DRAG prefactor as well as constant detuning, when accounting for time-ordering, and also show how to calibrate other prefactors for further performance improvement. Upon correcting these varied sources of error, we numerically demonstrate gate infidelities below 10^{-5} for a 7ns π -rotation when incorporating existing decoherence rates.

I. INTRODUCTION

Superconducting quantum circuits [1, 2] position themselves as a promising quantum computing platform due to the capacity of tailoring internal circuit parameters, enabling a high degree of controllability over individual qubits. Current quantum processing units based on transmon circuits [3] are described as anharmonic oscillators suffering from low anharmonicity, which induces transitions with the outlying energy levels through the drive, leading to accumulated population in non-computational states – leakage – and phase errors, upper-bounding the performance of the single-qubit operations [4].

The standard approach to correct these errors relies on using pulse shaping and is known as Derivative Removal by Adiabatic Gate (DRAG) [5–7], where an off-phase quadrature drive is added to the pulses to counteract leakage [5] and/or phase errors perturbatively [8]. However, this method has not been successfully employed when the driving amplitude becomes commensurate with the detuning, the so-called strong driving regime. Here, a crossover occurs where the three-level model of the transmon (or other anharmonic oscillator) breaks down, invalidating existing approaches in the literature. That is, as one tries to further speed up gates and improve system function, the driving amplitude approaches the anharmonicity of the ladder structure, and the dynamics becomes overconstrained with multiple leakage channels being activated [9, 10]. While several semi-classical mitigation strategies have emerged to add Fourier spectrum notches to unwanted transitions [11, 12], the semi-classical analysis is valid only in the perturbative regime.

In this work, we show that the above-mentioned semi-classical analysis and a three-level manifold are both insuf-

ficient to model the onset of the strong driving regime. We identify two-photon transitions that become dominant when only the linear drive term is corrected. By designing DRAG-type corrections that simultaneously target single- and two-photon leakage channels, through a recursive construction, we derive fully analytical pulse shapes that eliminate all leading error terms. In particular, we observe that a minimum four-level description is essential for capturing the necessary dynamics. Using these analytical pulses without any calibration, we achieve an error rate of 10^{-5} with an 11.8 ns gate.

In practice, free parameters are often introduced into the control terms and are calibrated to compensate for model uncertainties and further enhance the performance. These are often chosen in an ad-hoc manner, but exhibit correlated behaviour [4]. We explain the typically seen functional forms using toggling-frame transformations and a Magnus-expansion analysis, which together clarify where parameter calibration yields substantial improvements. In particular, we explain the linear relationship between detuning and the DRAG prefactor, and explain why, counterintuitively, constant detuning can outperform time-dependent detuning in several important cases. Incorporating additional prefactors to the recursive DRAG terms for calibration reduces the minimum achievable gate time further to 6.7 ns with error 10^{-5} .

The remainder of the paper is organized as follows: Sec. II A introduces the DRAG formalism and the first-order errors on single-qubit gates. Section II C describes the recursive DRAG approach, termed as R1D, for correcting two-photon errors $|0\rangle \rightleftharpoons |2\rangle$. Sec. II D generalizes to a second recursive set of frame transformations, termed as R2D, that further remove errors from the higher excited states of the ladder. Sec. III provides analytical predictions and analysis for the drive amplitude and constant detuning to remove additional computational-space errors. In Sec. IV, we analyse the effect of decoherence on the gate performance. Finally, in Sec. V we provide our conclusions.

* j.da.costa.jesus@fz-juelich.de

II. ERROR BUDGET AND CORRESPONDING CORRECTIONS

A. Linear leakage error and standard DRAG correction

We start by revisiting the DRAG method introduced in Ref. [5], considering a weakly anharmonic oscillator with four levels, $|0\rangle$, $|1\rangle$, $|2\rangle$ and $|3\rangle$, as depicted in Fig. 1(a). The first two levels are used for information processing – they form the computational subspace – with the rest representing leakage states. DRAG aims to implement operations between the lowest two levels while suppressing leakage and phase errors by engineering the drive envelope. Let us start with our system Hamiltonian in the rotating frame with respect to the drive frequency, taking $\hbar = 1$ (see Appendix A for a full derivation):

$$\hat{\mathcal{H}}(t) = \sum_{j=1}^M [\Delta_j + j\delta(t)]|j\rangle\langle j| + \sum_{j=1}^M \lambda_j \left[\frac{\Omega_x(t)}{2} \hat{\sigma}_{j-1,j}^x + \frac{\Omega_y(t)}{2} \hat{\sigma}_{j-1,j}^y \right] \quad (1)$$

where Δ_j is the anharmonicity of the j th level, $\delta(t)$ is a time-dependent detuning to be determined later and λ_j denotes the relative drive strength between $|j\rangle \rightleftharpoons |j+1\rangle$. Without loss of generality, we assume $\lambda_1 = 1$. For transmon circuits [3, 13], we can approximate $\lambda_j \equiv \sqrt{j}$. The symbols $\Omega_x(t)$ [$\Omega_y(t)$] are the in-phase (out-of-phase) drive envelopes. Finally $\hat{\sigma}_{j,k}^x = |j\rangle\langle k| + |k\rangle\langle j|$ and $\hat{\sigma}_{j,k}^y = i(|j\rangle\langle k| - |k\rangle\langle j|)$ are the generalized Pauli operators acting on multi-level systems.

The goal is to implement an on-resonant interaction between the lowest two levels ($\Delta_1 = 0$) while avoiding any population transfer to higher levels. DRAG achieves this by moving to an effective frame in which the ancillary levels decouple from the computational subspace, and by determining the corresponding corrections to the drive envelopes. The Hamiltonian in this frame reads $\hat{\mathcal{H}}_1(t) = \hat{V}(t)\hat{\mathcal{H}}(t)\hat{V}^\dagger(t) + i\dot{\hat{V}}(t)\hat{V}^\dagger(t)$, where overdot represents derivative with respect to time. Ideally, the frame transformation \hat{V} is chosen such that $\hat{V}(t)\hat{\mathcal{H}}(t)\hat{V}^\dagger(t)$ becomes block diagonal, eliminating couplings between the computational subspace and the ancillary levels [14].

Because computing the exact \hat{V} is typically expensive, a perturbative Schrieffer–Wolff approach [15] is commonly used, though in some cases non-perturbative transformations are possible [6, 9, 15]. Let $\hat{S}_1(t)$ denote the generator of $\hat{V}(t)$, $\hat{V}(t) = \exp(\hat{S}_1(t))$. The transformed Hamiltonian to second order is

$$\hat{\mathcal{H}}_1(t) \approx \hat{\mathcal{H}}(t) + [\hat{S}_1(t), \hat{\mathcal{H}}(t)] + \frac{1}{2!} [\hat{S}_1(t), [\hat{S}_1(t), \hat{\mathcal{H}}(t)]] + i\dot{\hat{S}}_1(t). \quad (2)$$

The generator $\hat{S}_1(t)$ generally corresponds to an anti-hermitian version of the interaction that we want to re-

move [14],

$$\hat{S}_1(t) = -i \sum_{j=1}^M \lambda_j \frac{\Omega_x(t)}{2\Delta_2} \hat{\sigma}_{j-1,j}^y. \quad (3)$$

Substituting this into Eq. (2), expanding to second order in Ω_x/Δ_2 , truncating to the lowest four levels and maintaining only the computational subspace and its transitions yields :

$$\begin{aligned} \hat{\mathcal{H}}_1(t) = & \frac{\Omega_x}{2} \hat{\sigma}_{0,1}^x + \left[\frac{\Omega_y}{2} + \frac{\dot{\Omega}_x}{2\Delta_2} \right] (\hat{\sigma}_{0,1}^y + \lambda_2 \hat{\sigma}_{1,2}^y) \\ & + \left[\delta(t) + \frac{(4 - \lambda_2^2)}{4\Delta_2} \Omega_x^2 \right] |1\rangle\langle 1| + \frac{\lambda_2 \Omega_x^2}{8\Delta_2} \hat{\sigma}_{0,2}^x \\ & - \Omega_x^2 \left[\frac{(2\Delta_2 - \Delta_3)}{8\Delta_2^2} \right] \lambda_2 \lambda_3 \hat{\sigma}_{1,3}^x + O\left(\frac{\Omega_x^3}{\Delta_2^2}\right) + \dots, \end{aligned} \quad (4)$$

where we omit time-dependency for simplicity. We maintain this approximation order, $O(\Omega_x^3/\Delta_2^2)$, in the Hamiltonians throughout this paper and consider only the qubit subspace and its transitions.

Eq. (4) is central to our analysis, as it identifies the dominant error mechanisms. The leading error arises from the linear coupling term $\hat{\sigma}_{1,2}^y$ with transition frequency Δ_2 which motivates the standard DRAG correction $\Omega_y(t) = -\dot{\Omega}_x(t)/\Delta_2$ [5] as depicted in Fig. 1(b), where we see the dominant error channels in the rotating frame with respect to the transition frequency ω . The phase accumulated on $|1\rangle$ can be removed by dynamically modulating the detuning following the relation $\delta(t) = -\Omega_x^2(4 - \lambda_2^2)/(4\Delta_2)$. In practice, this is often approximated by a constant detuning shift [4, 8]. Applying these corrections yields

$$\hat{\mathcal{H}}_1(t) \approx \frac{\Omega_x}{2} \hat{\sigma}_{0,1}^x + \frac{\lambda_2 \Omega_x^2}{8\Delta_2} \hat{\sigma}_{0,2}^x - \Omega_x^2 \left[\frac{(2\Delta_2 - \Delta_3)}{8\Delta_2^2} \right] \lambda_2 \lambda_3 \hat{\sigma}_{1,3}^x. \quad (5)$$

The remaining leakage channels are thus the two-photon processes $\hat{\sigma}_{0,2}^x$ and $\hat{\sigma}_{1,3}^x$. These contributions are negligible for weak drives but become significant as the gate time is reduced and Ω_x/Δ_2 increases, as illustrated in Fig. 1 (d), where a significant leakage to $|2\rangle$ and $|3\rangle$ can be observed for a DRAG pulse at 6ns. In the following subsections, we focus on mitigating these higher-order leakage terms.

B. Rotation angle and fidelity metric

Before proceeding, we first consider the constraints on the initial pulse shape prior to applying the DRAG correction. In general, we require the pulse to be smooth and vanish at both its beginning and end. This leads to the conditions

$$\int_0^T \Omega_x(t) dt = \theta, \quad (6a)$$

$$\Omega_x(0) = \Omega_x(T) = \dot{\Omega}_x(0) = \dot{\Omega}_x(T) = 0, \quad (6b)$$

which guarantee that the frame generated by $\hat{V}(t)$ coincides with the laboratory frame at the beginning and at the end of the

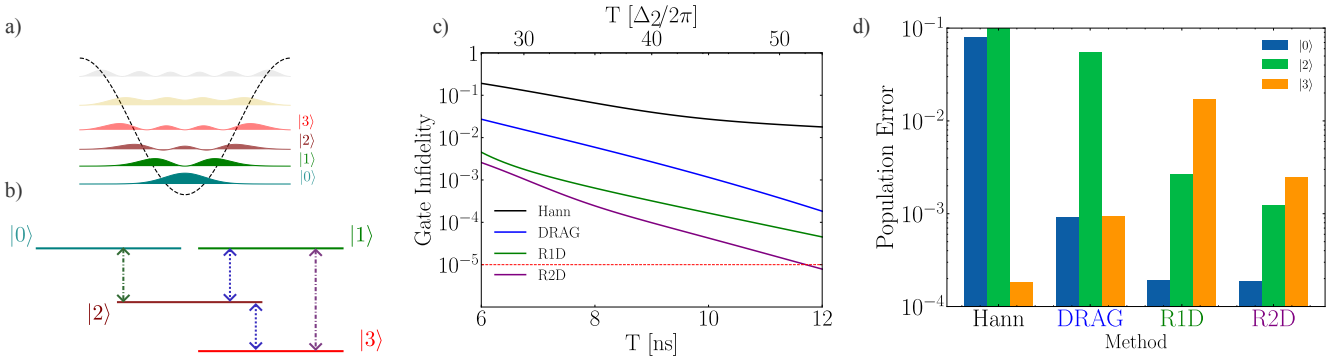


FIG. 1. **Analytical pulse performance for a transmon qubit.** a) Low-lying energy structure of a transmon system represented as a particle in a cosine potential, where different opacity refers to the importance of higher energy levels in the performance of the gate. b) Structure of the energy levels of the transmon system in the rotating frame with respect to the transition ω_{10} . The dashed arrows connecting different states represent single-photon transitions, while dotted dashed connects states through two-photon processes. c) Gate infidelity for implementing an X gate under different pulses: black lines corresponds to Hann pulse, blue line is for DRAG and green and violet stand for recursive pulses R1D and R2D, respectively. These pulses are simulated analytically without calibration. R2D outperforms every method and achieves a gate fidelity of 99.99 % at 9 ns and a fidelity of 99.999% at 11.8 ns. d) Histogram with the final population of the relevant leakage states for different pulses when implementing an X gate at 6ns. The main source of error in DRAG can be addressed by using R1D, which will suppress 2 photon transitions to $|2\rangle$. However, for R1D the leakage to $|3\rangle$ is a major source of error. This can suppressed by an order of magnitude by R2D. The simulations were performed by modeling the transmon as an anharmonic oscillator with anharmonicity $\Delta_2 = -2\pi \times 0.225$ GHz.

dynamics. To benchmark gate performance, we compute the average gate infidelity defined as $\mathcal{E}(\hat{\mathcal{U}}_Q) = 1 - \mathcal{F}[\hat{\mathcal{U}}_Q]$ where $\mathcal{F}[\hat{\mathcal{U}}_Q]$ can be found in Appendix B, following closely [16].

We compare different implementations using the Hann pulse $\Omega_{\text{Hann}}(t) = \Omega_0 \sin^2(\pi t/T)$ and the DRAG pulse $\Omega_{\text{DRAG}}(t) = \Omega_{\text{Hann}}(t) - i\dot{\Omega}_{\text{Hann}}(t)/\Delta_2$ for different gate times T . In Fig. 1 (c), we can see the gate infidelity for both protocols, for an anharmonicity of $\Delta_2/2\pi = -0.225$ GHz. This value for anharmonicity is used for all simulations throughout this paper. We observe that linear DRAG outperforms the Hann pulse at every gate time, obtaining errors below 10^{-4} for times longer than ≈ 12.7 ns. However, for gate times shorter than ≈ 10 ns we see that the performance of DRAG falls sharply with fidelities below 99.9%, demonstrating that at shorter times additional leakage channels (two-photon transitions) are the leading sources of errors.

C. Virtual leakage $|0\rangle \rightleftharpoons |2\rangle$ and R1D pulse

As mentioned in the previous subsection, to obtain a shorter gate time without compromising on fidelity, we need to address multiple leakage pathways arising from two-photon transitions. To simultaneously mitigate these errors, we employ the DRAG method recursively [6, 7, 9], where each successive frame transformation targets a specific leakage channel.

To eliminate the first two-photon process $\hat{\sigma}_{0,2}^x$, we move to a frame generated by $\hat{S}_2(t) = -i\lambda_2\Omega_1^2/(8\Delta_2^2)\hat{\sigma}_{0,2}^y$, where Ω_1 is a new trial waveform, and which changes the Hamiltonian to

$$\hat{\mathcal{H}}_2(t) \approx \hat{\mathcal{H}}_1(t) + \frac{\lambda_2\dot{\Omega}_1\Omega_1}{4\Delta_2^2}\hat{\sigma}_{0,2}^y - \frac{\lambda_2\Omega_1^2}{8\Delta_2}\hat{\sigma}_{0,2}^x. \quad (7)$$

In principle, one may already introduce a correction, as in Ref. [9]. However, this will generate a large out-of-phase component and complicate the gate calibration. Instead, we apply an additional virtual correction proportional to $\hat{\sigma}_{0,2}^y$, via $\hat{S}_3 = i\lambda_2\dot{\Omega}_1\Omega_1/(4\Delta_2^3)\hat{\sigma}_{0,2}^x$, that renders the resulting term real [6, 17] leading to

$$\hat{\mathcal{H}}_3(t) \approx \hat{\mathcal{H}}_1(t) - \lambda_2 \left[\frac{\dot{\Omega}_1^2 + \ddot{\Omega}_1\Omega_1}{4\Delta_2^3} + \frac{\Omega_1^2}{8\Delta_2} \right] \hat{\sigma}_{0,2}^x. \quad (8)$$

Collecting all terms involving $\hat{\sigma}_{0,2}^x$ and setting them to zero yields the first recursive correction (R1D) pulse:

$$\Omega_x(t) = \sqrt{\Omega_1^2 + \frac{2}{\Delta_2^2}(\dot{\Omega}_1^2 + \ddot{\Omega}_1\Omega_1)}. \quad (9)$$

We require that the R1D pulse satisfies the boundary conditions given in Eq. (6b). By direct inspection, $\Omega_x(t)$ vanishes at $t = 0$ and $t = T$, provided that Ω_1 obeys the same boundary conditions. However, $\dot{\Omega}_x(t)$ also needs to vanish at $t = 0$ and $t = T$, which imposes a new constraint on $\Omega_1(t)$. Evaluating

$$\lim_{t \rightarrow 0} \dot{\Omega}_x = \lim_{t \rightarrow 0} \frac{\Omega_1 + \frac{1}{\Delta_2^2}(3\ddot{\Omega}_1 + \ddot{\Omega}_1 \frac{\Omega_1}{\Delta_2^2})}{\sqrt{(\frac{\Omega_1}{\Delta_2^2})^2 + \frac{2}{\Delta_2^2}(1 + \dot{\Omega}_1 \frac{\Omega_1}{\Delta_2^2})}} \text{ and using}$$

$\lim_{t \rightarrow 0} \Omega_1(t)/\dot{\Omega}_1(t) = 0$, the expression reduces to $\lim_{t \rightarrow 0} \dot{\Omega}_x = 3\ddot{\Omega}_1/\sqrt{2\Delta_2^2}$. Thus satisfying the boundary conditions requires $\ddot{\Omega}_1(0) = \ddot{\Omega}_1(T) = 0$. The Hann pulse does not meet this additional condition, so instead we use $\Omega_1(t) = \Omega_0 \sin^3(\pi t/T)$. Relying on a higher power in the sinusoidal envelope does however sharpen the pulse in the time domain, which in turn broadens its frequency spectrum and potentially increases spectral content in unwanted transitions if no correction terms are added.

Using R1D, we implement a π -rotation along the x axis. Fig. 1(c) shows the gate infidelity as a function of T . As can be seen, this technique outperforms standard DRAG for all times, but especially for extremely fast gates, achieving a gate fidelity above 99.99% for gate times longer than ≈ 10.8 (ns), a 15% improvement in minimum gate time.

D. Virtual leakage $|1\rangle \rightleftharpoons |3\rangle$ and R2D pulse

The remaining bottleneck arises from leakage to $|3\rangle$, a two-photon process that has not been previously analyzed. After inserting the first recursion, the Hamiltonian reads

$$\hat{\mathcal{H}}_3(t) \approx \frac{\Omega_x}{2} \sigma_{0,1}^x + \left[\frac{\lambda_2 \lambda_3 (\Delta_3 - 2\Delta_2)}{8\Delta_2^2} \right] \Omega_x^2(t) \sigma_{1,3}^x. \quad (10)$$

To suppress this remaining transition, we introduce a second recursive DRAG (R2D), targeting the $|1\rangle \rightleftharpoons |3\rangle$ transition.

Because Ω_x has already been defined as a functional of Ω_1 , the next recursion must update Ω_1 itself. Directly doing so is challenging due to the derivative terms introduced by Eq. (9). We therefore perform a sequence of virtual transformations to eliminate these derivative contributions, which are frame transformations that do not modify the pulse shape. We introduce Schrieffer-Wolff generators with yet a new trial waveform Ω_V so that

$$\hat{S}_4(t) = -i\lambda_2 \lambda_3 \frac{\Omega_V^2 (\Delta_3 - 2\Delta_2)}{8\Delta_3 \Delta_2^2} \hat{\sigma}_{1,3}^y, \quad (11a)$$

$$\hat{S}_5(t) = i\lambda_2 \lambda_3 \frac{(\dot{\Omega}_V \Omega_V) (\Delta_3 - 2\Delta_2)}{(8\Delta_2^2 \Delta_3^2)} \hat{\sigma}_{1,3}^x, \quad (11b)$$

which together yield:

$$\begin{aligned} \hat{\mathcal{H}}_4(t) &\approx \hat{\mathcal{H}}_3(t) \\ &+ \lambda_2 \lambda_3 (2\Delta_2 - \Delta_3) \left[\frac{\dot{\Omega}_V^2 + \ddot{\Omega}_V \Omega_V}{8\Delta_2^2 \Delta_3^2} + \frac{\Omega_V^2}{16\Delta_2^2} \right] \hat{\sigma}_{1,3}^x. \end{aligned} \quad (12)$$

The role of these transformations is to eliminate derivatives of Ω_1 in the $|1\rangle \rightleftharpoons |3\rangle$ transition, leading to the constraint

$$2\Delta_3^2(\dot{\Omega}_1^2 + \ddot{\Omega}_1 \Omega_1) - \Delta_2^2(2\dot{\Omega}_V^2 + 2\ddot{\Omega}_V \Omega_V + \Delta_3^2(\Omega_V^2 - \Omega_1^2)) = 0. \quad (13)$$

Choosing $\Omega_V = \Delta_3 \Omega_1 / \Delta_2$ reduces the only remaining coupling term in $\hat{\mathcal{H}}_4(t)$ to a single Ω_1^2 term.

$$\hat{\mathcal{H}}_4(t) \approx \frac{\Omega_x}{2} \sigma_{0,1}^x + \lambda_2 \lambda_3 \Omega_1^2 \frac{(2\Delta_2 - \Delta_3)(\Delta_3^2 - \Delta_2^2)}{8\Delta_2^4} \hat{\sigma}_{1,3}^x. \quad (14)$$

We now eliminate this term using a second recursive transformation using trial waveform Ω_2 , given by the generators

$$\hat{S}_6(t) = -i\lambda_2 \lambda_3 \frac{\Omega_2^2 (2\Delta_2 - \Delta_3)(\Delta_3^2 - \Delta_2^2)}{(8\Delta_2^4 \Delta_3)} \hat{\sigma}_{1,3}^y, \quad (15a)$$

$$\hat{S}_7(t) = i\lambda_2 \lambda_3 \frac{\dot{\Omega}_2 \Omega_2 (2\Delta_2 - \Delta_3)(\Delta_3^2 - \Delta_2^2)}{(4\Delta_2^4 \Delta_3^2)} \hat{\sigma}_{1,3}^x, \quad (15b)$$

yielding the second recursive DRAG relation:

$$\Omega_1(t) = \sqrt{\Omega_2^2 + \frac{2}{\Delta_3^2} (\dot{\Omega}_2^2 + \ddot{\Omega}_2 \Omega_2)} \quad (16)$$

As before, we must determine the boundary conditions for the new trial pulse Ω_2 . We obtain that $\lim_{t \rightarrow 0} \ddot{\Omega}_1 = 3\ddot{\Omega}_2 / \sqrt{2\Delta_3^2}$ which requires $\ddot{\Omega}_1(0) = \ddot{\Omega}_1(T) = 0$. A possible solution is $\Omega_1(t) = \Omega_0 \sin^4(\pi t/T)$.

E. Starting pulse shape

Because of the sharpness of the new pulse envelope, we expect its frequency spectrum be broader and address other leakage transitions. Likewise, the higher the power in the pulse envelope, the larger the amplitude and consequently the higher order terms revealed by the DRAG frame may result in no improvement on the gate fidelity. However, this is not a limiting factor of the framework, instead it forces us to make an adequate selection of the initial pulse envelope that satisfies all the required boundary conditions and at the same time limits the maximal drive amplitude as much as possible. To this end, we use the pulse proposed in Ref. [10],

$$\Omega_I(t) = \Omega_{\text{Max}} \left[\frac{1}{16} \cos \frac{6\pi}{T} t - \frac{9}{16} \cos \frac{2\pi}{T} t + \frac{1}{2} \right]. \quad (17)$$

It is straightforward to demonstrate that $\Omega_I(t)$ satisfies all the boundary conditions required by both R1D and R2D. Moreover, this pulse has the advantage that the maximal amplitude is smaller than the extension of the Hann pulse as $\sin^4(\pi t/T)$.

Fig. 1 (d) shows the error budget for the different pulses, and that for ultra-fast gates, it becomes apparent the need to remove the $|1\rangle \rightleftharpoons |3\rangle$ transition. If we do not remove it, this becomes the limiting factor. By using the second square root we can obtain a decrease by an order of magnitude in the population of $|3\rangle$.

F. Superlinear corrections on the qubit manifold

We have demonstrated that it is possible to systematically reduce the error for single-qubit gates by including different recursions of the DRAG framework leading to significant error reduction. However, it is possible to reduce the error even more, achieving fidelities around 99.999%, by including corrections that involve higher order contributions to the X and Y component of the pulses. These corrections are obtained by expanding $\hat{\mathcal{H}}_1(t)$ [Eq. (4)] up to third order in Ω_x/Δ_2 , whose form is shown explicitly in Appendix C, Eq. C1.

To avoid over/under rotation on the computational subspace, we need to modify the pulse envelope to cancel the higher order correction by updating the pulse with

$$\Omega'_x(t) = \Omega_x(t) - \frac{(4 - \lambda_2^2) \Omega_x^3(t)}{8\Delta_2^2}. \quad (18)$$

The remaining higher order terms in $|1\rangle \leftrightarrow |2\rangle$ can be removed by changing the Y component of the pulse, which needs to be updated according to the effective Hamiltonian obtained through the transformation:

$$\hat{S}_5(t) = -i \sum_{j=1}^m \frac{\lambda_j}{2} \left[\frac{\Omega_x}{\Delta_2} + \frac{A}{\Delta_2^3} \right] \hat{\sigma}_{j-1,j}^y \quad (19)$$

where A is an auxiliary variable defined in Appendix C Eq. C2.

To remove both the Y component introduced in the pulse and the Stark-shift we perform the following pulse updates:

$$\Omega'_y(t) = -\frac{\dot{\Omega}'_x(t)}{\Delta_2} - \frac{\dot{A}}{\Delta_2^3}, \quad \delta' = \delta - \frac{A\Omega_x}{\Delta_2^3}. \quad (20)$$

These corrections in Eq. (18 and 20) are not exclusive to R2D and can be performed to every DRAG framework. In practice, they can also be corrected by optimizing the amplitude of pulses in experiments. Therefore, the corrections were included in all frameworks in Fig. 1 (c) to demonstrate a fair comparison of all methods under such higher order optimization. Note that for linear DRAG these expressions simplify substantially and $A = (4 - \lambda_2^2)\Omega_x^3(t)/(8\Delta_2^2)$. This can be implemented by using Ω'_x and simply taking $\Omega'_y(t) = -\dot{\Omega}_x(t)/\Delta_2$ and therefore no Y correction is necessary.

Using the corrected R2D pulse, we obtain errors an order of magnitude smaller than standard DRAG above 6ns and R1D above 12ns. As can be seen in Fig. 1 (c), a fidelity of 99.999% is obtained for pulses from 12 ns.

After the correction, we obtain a remaining leakage term involving three-photon process in $|0\rangle \leftrightarrow |3\rangle$:

$$\begin{aligned} \hat{\mathcal{H}}(t) \approx & \frac{\lambda_1 \lambda_2 \Omega_x}{\Delta_2^4} \left[\frac{(\Delta_2^2 - \Delta_3^2)(\Delta_3 - 2\Delta_2)}{16\Delta_3} \Omega_2^2 + \right. \\ & \left. \frac{\Delta_2(3\Delta_2 - \Delta_3)\Omega_x^2 - 3(\Delta_3 - 2\Delta_2)(\Omega_1^2(\Delta_2 + \Delta_3))}{48} \right] \sigma_{0,3}^x \\ & - \frac{\lambda_1 \lambda_2 \Omega_x}{\Delta_2^4} \left[\frac{3(\Delta_3 - 2\Delta_2)\Omega_1 4i\dot{\Omega}_1}{48} \right] \sigma_{0,3}^y, \end{aligned} \quad (21)$$

this term is difficult to remove and cannot be easily simplified by virtual transitions due to the fact that all terms are proportional to Ω_x and Ω_x is dependent on $\ddot{\Omega}_1, \ddot{\Omega}_1 \dot{\Omega}_2, \ddot{\Omega}_2$.

G. Minimum Gate time

Given the square root in Eq.(9) and the fact that we require the pulse to be real, we have an extra condition on the minimal time required to complete a full rotation for an R1D pulse, $T_{\min} = \sqrt{6\pi}/\Delta_2$.

We can generalize this expression to several orders of recursion by assuming that the initial pulse has as shape $\Omega_1(t) = \Omega_0 \sin^n(\pi t/T)$ with the condition $\Omega_1^2(T_{\min}) + 2[\dot{\Omega}_1^2(T_{\min}) +$

$\ddot{\Omega}_1(T_{\min})\Omega_1(T_{\min})]/\Delta_2^2 = 0$. By replacing the argument of $\Omega_x(t)$ from Eq. (9), we get

$$\left[1 - \frac{2n\pi^2}{\Delta_2^2 T_{\min}^2} \right] \sin^2 \left[\frac{\pi t}{T_{\min}} \right] + \frac{2n(2n-1)\pi^2}{\Delta_2^2 T_{\min}^2} \cos^2 \left[\frac{\pi t}{T_{\min}} \right] = 0. \quad (22)$$

Notice that we need to guarantee that this expression is positive for all times. However, we know that the minimum of Eq. (22) is achieved when $t = T_{\min}/2$, reducing the expression to

$$T_{\min} = \sqrt{2n} \frac{\pi}{\Delta_2}. \quad (23)$$

For the R2D pulse, we require that both square roots remain positive. Following the same procedure as above we obtain the following:

$$T_{\min} = \frac{\pi \sqrt{n(\Delta_2^2 + \Delta_3^2) + \sqrt{n^2(\Delta_2^4 + \Delta_3^4) + (4 - 10n)n\Delta_2^2\Delta_3^2}}}{\Delta_2\Delta_3} \quad (24)$$

which reduces to the previous equation under the assumption $\Delta_3 \gg \Delta_2$. This leads us to the interesting and unexpected finding that, for the same Δ_2 , the minimum gate time T_{\min} for R2D increases with increasing Δ_3 , that is, the bigger the separation between $|2\rangle$ and $|3\rangle$ for the same anharmonicity, the slower the gate.

The minimum gate time for R1D and R2D using the pulse in Ref. [10] is obtained by ensuring both square roots are positive. This can be solved numerically and, for an anharmonicity of $\Delta_2/2\pi = -0.225$ GHz gives us a gate time of ≈ 4.45 [ns].

III. PREFACTOR VALUES FROM ANALYTICAL TIME-ORDERING AND NUMERICAL OPTIMIZATION

It is now common practice to optimize the coefficient for linear DRAG in single qubit gates [4, 18]. Yet the underlying physics governing these optimized corrections is seldom clarified. This gap arises both from discrepancies between the idealized model and the actual device, such as parameter drift [19–21], distortion on the pulses [22, 23], crosstalk [17], and from the presence of additional destructive interference pathways among different error channels. While treating the calibration as a black-box optimization has enabled state-of-the-art fidelities, further progress requires a deeper understanding of the dynamics.

In this section, we analyze the role of each free parameter and develop a systematic framework for Hamiltonian engineering. Our analysis reveals how these parameters interact, identifies which error channels they influence, and provides analytical expressions for their near-optimal values.

A. Parameterization of DRAG solution families

For linear DRAG, a set of parameters is given by the triad $\{\beta, \alpha, \delta_c\}$, first introduced in [8], that appears in the control as

$$\Omega \rightarrow \beta(\Omega_x + \alpha\Omega_y), \quad \delta \rightarrow \delta_c. \quad (25)$$

where β parameterises changes in the total amplitude and α ratio for the Y component. The parameter δ_c is a constant detuning correction due to frequency mismatch between the carrier frequency of the drive and the real transition frequency of the system, introduced by the Stark shift. This set of parameters follows the one used in Ref. [4].

Fig. 2 compares the gate infidelity $\mathcal{E}(\hat{\mathcal{U}}_Q)$ as a function of the gate time for different pulses. We observe that the optimized version of linear DRAG always outperforms the analytical one for gate times longer than 6 ns. We find that around 9.1 ns we have a destructive interference between the remaining uncorrected leakage channels, such that we can eliminate all leakage remaining. This way, between $T = 8.93$ ns and $T = 9.32$ ns we achieve the threshold of error below 10^{-5} , assuming sufficiently low decoherence. Moreover, the numerical optimization exhibits quasi-periodic peaks that are monotonically decreasing in the gate fidelity, where presumably some sort of destructive interference behaviour decreases the gate infidelity, reaching the numerical precision. Note however that picking the precise time duration for a low-infidelity gate is known [24] to be problematic for a number of reasons. Aside from pulse timing errors, the calibration process becomes much more cumbersome as in addition to the calibration of the pulse parameters, the gate duration must also be calibrated. In a multi-qubit processor, these optimal durations will moreover vary from qubit to qubit, which prohibits a common clock frequency for the processor, rendering quantum circuits highly cumbersome. Therefore, one cannot in general count on such an approach for ultra-low error.

To understand the underlying physics behind these parameters we modify Eq. (3) to consider a continuous set of adiabatic transformation given by [8]

$$\hat{S}_D(t) = -i\lambda_1 \frac{\alpha\Omega_x}{2\Delta_2} \hat{\sigma}_{0,1}^y - i \sum_{j=2}^m \lambda_j \frac{\Omega_x}{2\Delta_2} \hat{\sigma}_{j-1,j}^y. \quad (26)$$

We use this frame to ensure no terms proportional to $\hat{\sigma}_{0,1}^y$ remain in the computational subspace whilst removing the leakage term $\hat{\sigma}_{1,2}^x$.

B. Optimal detuning

We now look for the update to the triad $\{\beta, \alpha, \delta_c\}$ such that both leakage and phase errors cancel at the same time. To do so, we transform the starting Hamiltonian, Eq. (1), and expand to third order in $O(\Omega_x/\Delta)$, using the new frame generator, Eq. (26). Additionally, we move to the *toggling frame* [25, 26] given by the unitary which will represent ideal dynamics:

$$\hat{V}_{\text{Tog}}(\theta) = \exp(-i\theta\sigma_{0,1}^x + \phi_1|2\rangle\langle 2| + \phi_3|3\rangle\langle 3|) \quad (27)$$

where the rotation angle is given by $\theta(t) = \int_0^t \Omega_x(s)ds/2$ and ϕ_1 and ϕ_2 allow for free precession beyond the qubit

subspace. It is important to note that $\hat{V}_{\text{Tog}}(T) \neq I$, and in fact $\hat{V}_{\text{Tog}}(T)$ generates the desired π rotation. Therefore, the transformed toggling Hamiltonian will represent the error of our gate. If $H_{\text{Tog}} = 0$ for all time, the π rotation can be ideally implemented.

The goal of the toggling transformation is to separate the error part of the dynamics H_{Tog} , which is typically small. This ensures fast convergence of the Magnus expansion [24, 27, 28] which allows us to express the propagator as $\hat{T} \exp(-i \int_0^T \hat{\mathcal{H}}(t)dt) = \exp(-i \sum \hat{\mathcal{Z}}_\ell(t))$, where $\hat{\mathcal{Z}}_\ell(t)$ are the different orders of the expansion defined as

$$\hat{\mathcal{Z}}_1(t) = \int_0^T dt \hat{\mathcal{H}}(t), \quad (28a)$$

$$\hat{\mathcal{Z}}_2(t) = \int_0^T dt \int_0^t d\tau [\hat{\mathcal{H}}(t), \hat{\mathcal{H}}(\tau)], \quad (28b)$$

Thus, we shall find the conditions for the parameters introduced in the toggling frame to make $\hat{\mathcal{Z}}_1(t)$ close to 0 as possible. This leads to equations for the phase and rotation error in the qubit subspace [explicitly given as Eq. (D1) and Eq. (D2) respectively in Appendix D] that we wish to make 0.

For π rotation, the phase error turns out to be trivially zero because of symmetry. Given the rotation angle $\theta = \int \frac{2\pi}{T} \sin^2(\pi\tau/T)$, then $\cos \theta$ will be an odd function over the period of integration $[0, T]$ around $T/2$. This simplifies the first term in Eq. (D1) to zero – we only have products of con-

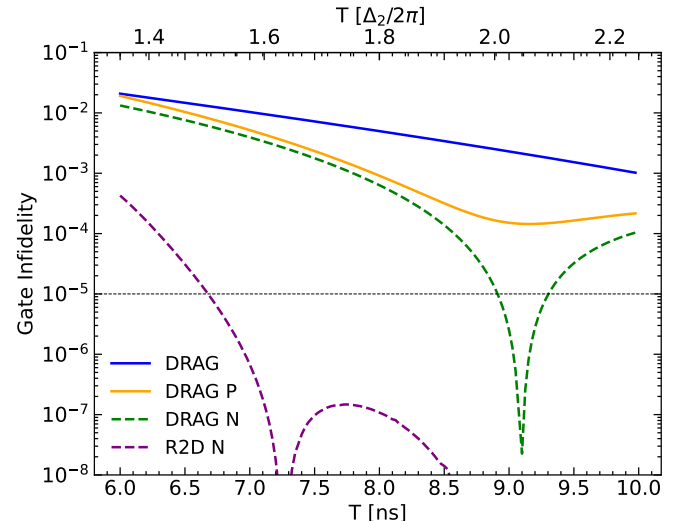


FIG. 2. **Gate performance under different pulse protocols.** Gate infidelity as a function of Gate time for analytical linear DRAG (blue), linear DRAG using the predictions for α, β and δ_c (DRAG P, orange), linear DRAG with optimized parameters (DRAG N, green) and R2D with optimized parameters, $\alpha_{12}, \alpha_{02}, \alpha_{13}, \beta$ and δ_c (R2D N, purple). Despite the mismatch between the predictions for α for linear DRAG and the optimized values, we obtain a significant improvement on the fidelity of the gate demonstrating that parametrized constants can eliminate higher order errors. The parameterized R2D pulse outperforms all others for all gate times considered, achieving a fidelity of 99.999% at 6.70 ns, a $\approx 25\%$ improvement versus standard DRAG (which reaches 99.999% fidelity at 8.93 ns.)

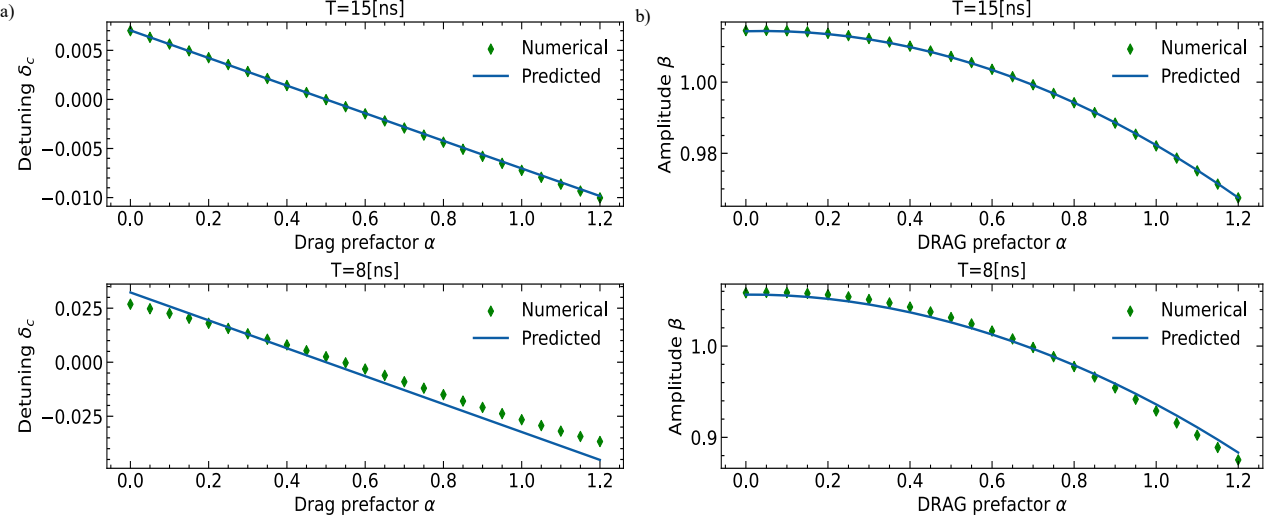


FIG. 3. **Amplitude and Constant Detuning as a function of α** a) Comparison between the optimized values of constant detuning δ_c for the DRAG pulse and the analytical approximation, for different values of α . The analytical expression can accurately predict the values of constant detuning. The longer the gate time, the better the prediction. b) Comparison between the optimized values of β for the DRAG pulse and the analytical approximation, for different values of α . Once again, the analytical expression can accurately predict the values of constant detuning.

stants and odd functions or even functions and odd functions. The same logic applies to the second component where now $\sin \theta$ is even but $\dot{\Omega}_x$ is odd. This way we can use the constant detuning δ_c and the amplitude of the pulse to make Eq. (D1) = 0. It is important to note that this is only true for the π rotation. In general, one would not be able to make both equations zero using constant detuning. A time-dependent detuning, like the one used in Section II would be required. This also explains why using the DRAG formula with constant detuning for partial rotation is often seen to have larger error than one would naively expect given the proportionate reduction in pulse amplitude.

The requirement that Eq. (D2) = 0 now gives us the tools to predict the value of the constant detuning and the amplitude of the pulse. Starting with zeroing the imaginary part gives the equation for δ_c :

$$\delta_c = -\frac{\int_0^T (4\alpha - \lambda_2^2) \Omega_x^2 \sin \theta}{\int_0^T 4\Delta_2 \sin \theta} - \frac{\int_0^T \dot{\Omega}_x (\alpha - 1) \alpha \lambda_2^2 \Omega_x \cos \theta}{\int_0^T 8\Delta_2^3 \sin \theta}. \quad (29)$$

Note that this is not just an average of the accumulated time-dependent Stark shift, but is renormalized by the rotation angle θ . Assuming a pulse shape of the form $\Omega_x = 2\pi \sin^2(\pi t/T)/T$ we get:

$$\delta_c \approx 0.712 \frac{\lambda_2^2 - 4\alpha}{\Delta_2} \frac{\pi^2}{T^2}. \quad (30)$$

Fig. 3 (a) compares the analytical expression using Eq. 30 with numerically optimized results for different DRAG coefficient α and two different gate times $T=8$ ns and $T=15$ ns. The level of agreement is governed by the Magnus expansion: as the gate time increases, higher-order terms become

negligible, and the analytical and numerical results converge. The constant detuning expression also explains the physics observed in the experimental realization in Ref. [4], where a linear relationship between α and δ_c was reported with $\delta_c = 0$ roughly at $\alpha = 0.5$ (for $\lambda_2 \approx \sqrt{2}$) [8]. The experiment also observed scaling $\delta_c \propto 1/T^2$, which is verified by our analysis. Recent results in Ref. [29] further confirm the strong agreement between this analytical expression and calibrated constant-detuning values.

C. Optimal Rabi frequency

For the amplitude of the pulse, coming from the real part of Eq. (D2), we have the following term

$$\int_0^T \frac{\beta \Omega_x - \dot{\theta}}{2} - \frac{\beta \Omega_x (\Delta_2 8\alpha \delta_c + (4\alpha^2 + \lambda_2^2(1-2\alpha)\beta^2 \Omega_x^2))}{16\Delta_2^2} \quad (31)$$

which is a cubic polynomial of β and must be set to zero. Despite Eq. (31) having an analytical solution, it is quite cumbersome to solve. Instead, assuming a mean-field approximation as $\beta = 1 + \eta$ by considering a small variation of the expected optimal amplitude, we can linearize Eq. (31) as $\beta^3 \approx 1 + 3\eta$ leading to

$$\beta = 1 + \frac{16\alpha \delta_c \pi \Delta_1 + (4\alpha^2 + \lambda_2^2 - 2\alpha \lambda_2^2) \frac{5\pi^3}{T^2}}{16\pi \Delta_1^2 - 16\alpha \delta_c \pi \Delta_1 - 3(4\alpha^2 + \lambda_2^2 - 2\alpha \lambda_2^2) \frac{5\pi^3}{T^2}}, \quad (32)$$

corresponding to the correction of the drive amplitude as a function of the DRAG coefficient α for fixed gate time T . It also shows how one can correct the X superlinear correction

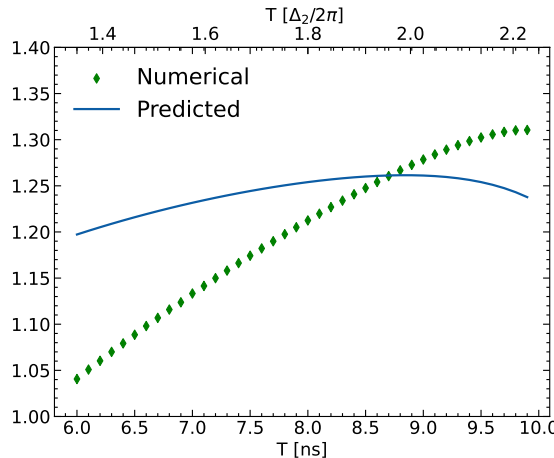


FIG. 4. **Analytically vs Numerically optimized α 's parameter.** Comparison between the optimized values of α for linear DRAG pulse and the analytical expression of α , as a function of gate time T . Although our expression captures the general behaviour of α , we find large discrepancies, most likely due to higher orders.

identified in section II F alternatively, through prefactor calibration.

Fig. 3 (b) compares the amplitude correction β obtained in Eq. (32) with the one obtained through numerical optimization at two different gate times. Just as in the previous case, the agreement between the analytical and the numerical results is conditioned on the validity of the first-order Magnus expansion and improves with gate times, and is generally extremely good.

D. Linear DRAG prefactor

Finally, to understand and predict the value of α we must look into $\hat{\mathcal{Z}}_1[1, 2]$ (and $\hat{\mathcal{Z}}_1[2, 1]$) and $\hat{\mathcal{Z}}_1[0, 2]$ (and $\hat{\mathcal{Z}}_1[0, 2]$) which represent the main leakage channel in our error Hamiltonian (and whose contributions came from a mixture of the $|1\rangle \leftrightarrow |2\rangle$ and $|0\rangle \leftrightarrow |2\rangle$ transitions in the lab frame). These elements can be found in Appendix D, Eq. D3 and Eq. D4.

In order to minimize the leakage we now want the α that minimizes $l = |\hat{\mathcal{Z}}_1[1, 2]|^2 + |\hat{\mathcal{Z}}_1[0, 2]|^2$. This can be found by taking the derivative $\partial l / \partial \alpha = 0$. To solve this equation, we approximate $\phi_\ell = \Delta_\ell t$, and we once again perform a mean field approximation, this time over the alphas $\alpha = (1 + \delta\alpha)$ such that $\alpha^n = (1 + n\delta\alpha)$.

Solving this equation we obtain the following expression for α :

$$\alpha \approx 1 - \frac{x_1 + \bar{x}_1}{x_2 + \bar{x}_2}, \quad (33)$$

with

$$\begin{aligned} x_1 &= h_{12}^1(\bar{h}_{12}^0 + \bar{h}_{12}^1 + \bar{h}_{12}^2) + 2h_{12}^2(\bar{h}_{12}^0 + \bar{h}_{12}^1 + \bar{h}_{12}^2) \\ &+ h_{02}^1(\bar{h}_{02}^0 + \bar{h}_{02}^1 + \bar{h}_{02}^2) + 2h_{02}^2(\bar{h}_{02}^0 + \bar{h}_{02}^1 + \bar{h}_{02}^2), \\ x_2 &= h_{12}^1\bar{h}_{12}^1 + 2h_{12}^1\bar{h}_{12}^2 + 2h_{12}^2\bar{h}_{12}^0 + 4h_{12}^2\bar{h}_{12}^1 + 6h_{12}^2\bar{h}_{12}^2 \\ &+ h_{02}^1\bar{h}_{02}^1 + 2h_{02}^1\bar{h}_{02}^2 + 2h_{02}^2\bar{h}_{02}^0 + 4h_{02}^2\bar{h}_{02}^1 + 6h_{02}^2\bar{h}_{02}^2, \end{aligned}$$

where the symbol h_{ij}^k represents the integral from 0 to T of the k th α power in $\hat{\mathcal{H}}_{\text{Tog}}[i, j]$, i.e. $\hat{\mathcal{Z}}_1[1, 2] = \int_0^T \hat{\mathcal{H}}_{\text{Tog}}[1, 2] dt = h_{12}^0 + h_{12}^1\alpha + h_{12}^2\alpha^2$ and \bar{x}_1 (\bar{x}_2) is the complex conjugate of x_1 (x_2).

Fig. 4 compares the analytical expression for α with values obtained from full numerical optimization. In principle, $\alpha = 1$ should completely compensate for the single-photon leakage channel $|1\rangle \rightleftharpoons |2\rangle$. The analytical prediction lies around 1.2, reflecting the trade-off between this channel and the concurrent $|0\rangle \rightleftharpoons |2\rangle$ transition. Numerical optimization reveals a steeper slope for the α -dependence, ranging from 1.0 to 1.3, which arises from higher-order, superlinear corrections not included in the analytical calculation.

With the prediction of all three parameters, we can now compare the performance between the predicted prefactors and those from full numerical optimization. As seen in Fig. 2, despite the discrepancy in the α , the predicted prefactors provide large improvements to gate fidelity, with more than 1 order of magnitude. The largest deviation in fidelity is observed around 9 ns, where destructive interference is present among different leakage channels. In this regime, numerical optimization achieves further gains because it fully explores these interference pathways by optimizing the final unitary directly.

E. Parameter optimization for recursive pulses

The same procedure can be applied to R2D. We replace α with 3 constants, α_{12} , α_{02} and α_{13} , each allowing for higher order corrections in the 1-2, 0-2 and 1-3 transitions, respectively. The introduction of these constants correspond to replacing α in Eq. (26) with α_{12} and changing the frame transformations: $\hat{S}_3 \rightarrow \alpha_{02}\hat{S}_3$ and $\hat{S}_7 \rightarrow \alpha_{13}\hat{S}_7$. This changes our pulses to:

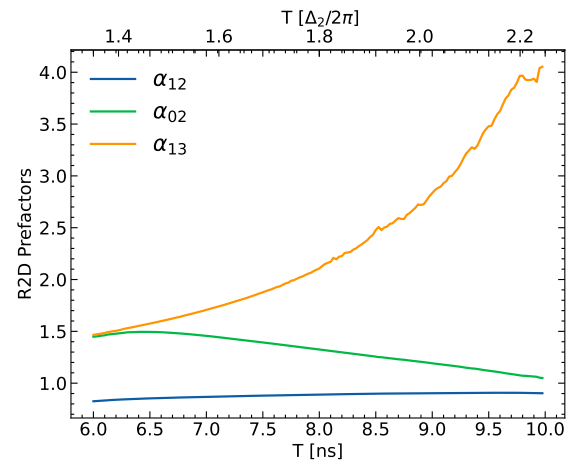


FIG. 5. **Numerically optimized α 's parameters.** Optimal values of α_{12} , α_{02} and α_{13} for the R2D pulse as a function of gate time T . These results generally match the ones obtained in experiment [29], validating the theory.

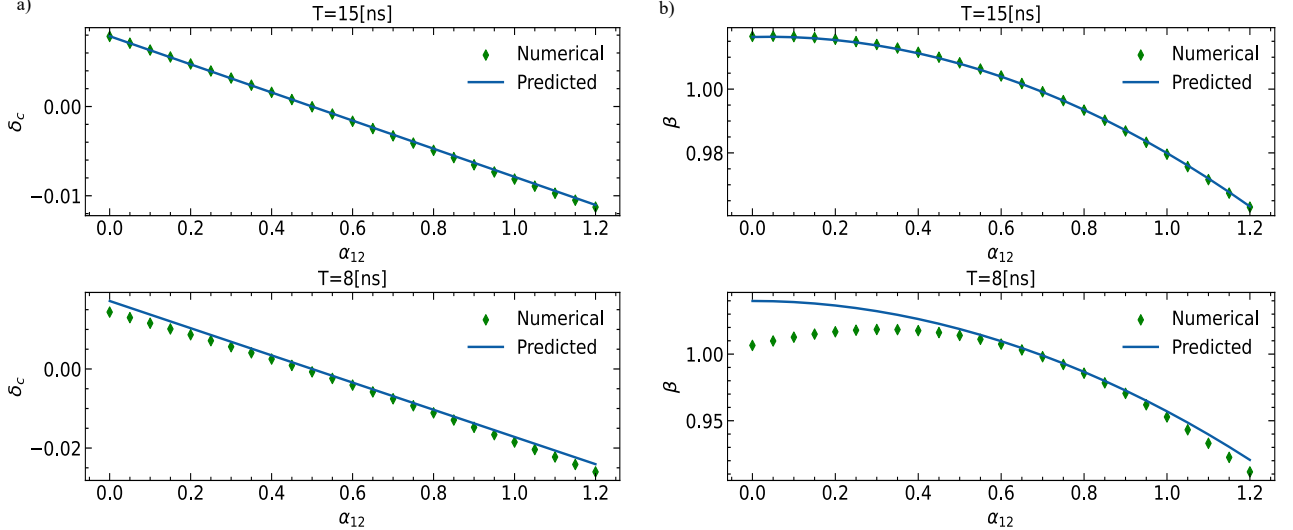


FIG. 6. **Amplitude and Constant Detuning as a function of α_{12}** a) Comparison between the optimized values of constant detuning for the R2D and the analytical approximation, for different values of α_{12} . To make this example, we chose $\alpha_{02} = 1.3$ and $\alpha_{13} = 1.7$. The analytical expression can accurately predict the values of constant detuning. The longer the gate time, the better the prediction. b) Comparison between the optimized values of β for the R2D pulse and the analytical approximation, for different values of α_{12} . Once again, the analytical expression can accurately predict the values of constant detuning.

$$\Omega_1(t) = \sqrt{\Omega_2^2 + \frac{2\alpha_{13}}{\Delta_3^2}(\dot{\Omega}_2^2 + \ddot{\Omega}_2\Omega_2)} \quad (34)$$

$$\Omega_x(t) = \sqrt{\Omega_1^2 + \frac{2\alpha_{02}}{\Delta_2^2}(\dot{\Omega}_1^2 + \ddot{\Omega}_1\Omega_1)}. \quad (35)$$

and

$$\Omega \rightarrow \beta(\Omega_x + \alpha_{12}\Omega_y), \quad \delta' \rightarrow \delta_c. \quad (36)$$

with $\Omega_2(t) = \sin^4 \pi t/T$. To second order in the error, $O(\Omega_x^2/\Delta_2^2)$, these parameters will be orthogonal and are free to eliminate higher order errors.

Fig. 2 shows the optimization of the gate infidelity as a function of time. As can be seen, we achieve significant improvements in fidelity, with a fidelity of 99.999 % achieved at $T \approx 6.78$ ns, demonstrating once again the capacity of correcting for higher order terms through calibrating constants. Contrary to linear DRAG, the fidelity stays above this threshold for all times beyond.

Unfortunately, analytical prediction of the three DRAG prefactors becomes intractable, as deviations in any one parameter feed back into the others through higher-order corrections, resulting in a coupled set of nonlinear equations. Nevertheless, we find a good agreement between our simulations and the experimental results obtained in [29]. The parameters can be found in Fig. 5. In contrast to α_{12} and α_{02} , α_{13} becomes bigger as time goes on because the maximum amplitude of the pulse becomes smaller with increasing α_{13} . This reduces all sources of error at higher orders (and therefore compensates the increase in the 2 photon leakage from $|1\rangle \leftrightarrow |3\rangle$).

For the amplitude and constant detuning, Eqs. (29) and (31) remain valid to the same order in $O(\Omega_x/\Delta)$, with the replacement rule $\alpha \rightarrow \alpha_{12}$, as can be seen in Fig. 6 (a) and (b). Interestingly enough, this means that the correction to the amplitude of the pulse and the constant detuning are mostly defined by α_{12} .

One final note regarding the optimization of R2D pulses – α_{02} and α_{13} will change the minimum gate time. In general, a numerical verification is necessary to extract a minimum gate time. However, if $\alpha_{02} > \alpha_{13}$, the expression for minimum gate time can be reduced to:

$$T_{min} = \frac{\pi \sqrt{n(\alpha_{13}\Delta_2^2 + \alpha_{02}\Delta_3^2) + \nu}}{\Delta_2\Delta_3}, \quad (37)$$

with

$$\nu = \sqrt{n^2(\alpha_{13}^2\Delta_2^4 + \alpha_{02}^2\Delta_3^4) + 2(2 - 5n)n\alpha_{13}\alpha_{02}\Delta_2^2\Delta_3^2}. \quad (38)$$

IV. DISSIPATIVE DYNAMICS

We calculate the system dynamics considering losses mechanisms including energy relaxation and dephasing. The evolution is described by the master equation in Lindblad form [30]

$$\dot{\rho}(t) = -i[\mathcal{H}(t), \rho(t)] + \gamma \mathcal{D}[\hat{a}]\rho(t) + \gamma_\phi \mathcal{D}[\hat{a}^\dagger \hat{a}]\rho(t), \quad (39)$$

where $\rho(t)$ is the density matrix of the system, $\mathcal{D}[\hat{O}] = O \bullet O^\dagger - \{O^\dagger O, \bullet\}/2$ is the Lindbladian super-operator and $\gamma = 1/T_1$ and $\gamma_\phi = 1/T_2^*$ correspond to the decay rates for

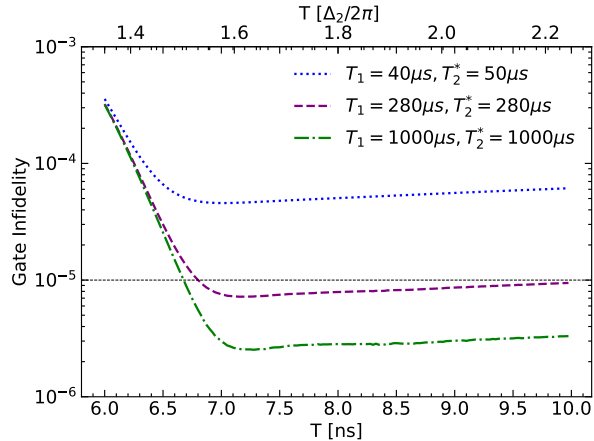


FIG. 7. **Gate averaged infidelities for a π gate using optimized parameters under decoherence.** As T_1 and T_2^* improves, R2D pulses manage to reach 99.999% fidelity.

energy losses and dephasing, respectively. We have chosen 2 sets of T_1 and T_2 , respectively (40,50) μ s and (280, 220) μ s, representing a range of values achievable today [31]. We also add a third set, (1000,1000) μ s, values which we hope will be reached in the near future. Finally, \hat{a} is the annihilation operator describing the transmon system. As the dissipative dynamics are state-dependent instead of unitary-dependent, we need to evaluate the gate performance for all the states of the Bloch sphere of the two-level system and average them [32].

As can be seen in Fig. 7, the R2D is capable of achieving a fidelity of 99.999% even under decoherence, for a gate time of $T = 6.93$ ns, with a minimum in infidelity at $T = 7.25$ ns. This demonstrates that single qubit gates with infidelities below 10^{-5} are possible in today's hardware.

V. SUMMARY AND CONCLUSION

In this work, we expand on the DRAG framework by including higher levels not usually considered and we show that these levels have a real impact on gate fidelity through multi-photon processes. Taking these in consideration, we extract new analytical expressions for pulses that show that it is possible to implement high-fidelity single-qubit gates at faster speeds and stronger driving strengths than previously considered.

We also explore numerical optimization of DRAG and R2D pulses. For the DRAG pulses we obtain theoretical approximations for the calibrating parameters, expressions that we hope will simplify and speed up normal calibration procedures. The obtained expressions for constant detuning are experimentally validated in [29]. For R2D pulses we show that a moderate optimization allows us to achieve high fidelity pulses faster, even under the effects of system decoherence, a critical step in enabling future quantum computation.

Although our equations were inspired by the transmon model, R2D is applicable for any ladder system modelled under the rotating wave approximation [6]. Future work is required to go beyond this approximation and to remove the re-

maining three-photon processes in the system.

Experimental implementation of this theoretical framework has been achieved by Y. Gao et al. [29], where R2D pulses were implemented and used to implement single qubit gates with suppressed two-photon leakage channels at world record speeds (6.8 ns) and drive strengths, Ω_x/Δ_2 , whilst maintaining a fidelity of 99.98%, limited by decoherence at that gate duration.

ACKNOWLEDGMENTS

We thank Manuel Guatto, Dimitrios Georgiadis, Shahrukh Chishti and Asier Galicia for valuable discussions. This work was funded by the Federal Ministry of Education and Research (BMBF) within the framework programme "Quantum technologies - from basic research to market" (Project QSolid, Grant No. 13N16149) and by Horizon Europe program via project QCFD (101080085, HORIZON-CL4-2021-DIGITAL-EMERGING02-10), project OpenSuperQ-Plus100 (101113946, HORIZON-CL4-2022-QUANTUM-01-SGA) and by the Cluster of Excellence Matter and Light for Quantum Computing (ML4Q2) EXC 2004/1 – 390534769.

Appendix A: Charge basis Hamiltonian

We start by deriving the effective Hamiltonian of a transmon circuit being driven on resonance with the $|0\rangle \rightleftharpoons |1\rangle$ transition. The transmon circuit oscillator is described by the Hamiltonian [3]

$$\hat{\mathcal{H}} = 4E_C[\hat{n} - n_g(t)]^2 - E_J \cos(\hat{\phi}) \quad (\text{A1})$$

where E_C and E_J represent the charge and Josephson energies, and $n_g(t)$ is the dimensionless gate voltage. The operator \hat{n} is the charge operator, indicating the number of Cooper pairs, and $\hat{\phi}$ denotes the phase operator. We can implement single-qubit operations by driving the circuit with an external source using $n_g(t) = n_0(t) \cos(\omega_d t)$ resulting in the Hamiltonian

$$\hat{H}_{\text{ctrl}} = \Omega(t) \cos(\omega_d t) \hat{n} \quad (\text{A2})$$

where $\Omega(t) = -8E_C n_0(t)$ is the complex drive envelope, and ω_d is the drive frequency. For the low-lying energy spectrum of this device, we can model it as an approximate Duffing oscillator [2, 13], where the controls now are given by $\hat{n} \propto (\hat{b}^\dagger + \hat{b})$, where \hat{b} is the annihilation operator of a linear oscillator. For the free energy term, we expand the cosine up to fourth order leading to

$$\hat{H}_0^{\text{duf}} = \omega_q \hat{b}^\dagger \hat{b} + \frac{\Delta}{2} \hat{b}^\dagger \hat{b}^\dagger \hat{b} \hat{b}, \quad (\text{A3})$$

with $\omega_q = \sqrt{8E_J E_C} - E_C$ and $\Delta = -E_C$. However, the eigenenergies and coupling strengths deviate from the Duffing model at higher levels due to the higher-order expansion of the cosine potential [13]. The accurate description of the transmon circuit requires diagonalize $\hat{\mathcal{H}}$ up to a truncation level N_{max} , which gives

$$H_0 = \sum_{k=0}^{N_{\text{max}}} \omega_k |k\rangle \langle k|, \quad (\text{A4})$$

whereas the charge operator takes the form

$$\begin{aligned} \hat{n} = & \sum_{k=0}^{N_{\text{max}}-1} \left[\lambda_{k,k+1} |k\rangle \langle k+1| \right. \\ & \left. + \sum_{j=1}^{\lambda_{k,k+2j+1}} |k\rangle \langle k+2j+1| \right] + \text{h.c.} \quad (\text{A5}) \end{aligned}$$

where λ denotes the corresponding matrix element. The maximal j is chosen such that $k+2j+1$ falls within the truncated levels. Unlike the Duffing oscillator model, the charge operator contains additional transitions corresponding to the underlying parity symmetry from the Mathieu functions. We can demonstrate that the coupling terms beyond the ladder structure are orders of magnitude smaller and are suppressed by the rotating-wave approximation.

From this point, it is more convenient to express the Hamiltonian in the rotating frame defined by the transformation

$R = \exp(-i\omega_d t \sum_k k |k\rangle \langle k|)$, where ω_d is the selected driving transition frequency. This leads to the following total Hamiltonian:

$$\begin{aligned} \hat{H} = & \sum_{k=0}^{N_{\text{max}}} \tilde{\Delta}_k |k\rangle \langle k| + \Omega(t) \cos(\omega_d t) \left[\right. \\ & \left. \sum_{k=0}^{N_{\text{max}}-1} \sum_{j=1}^{\lambda_{k,k+2j+1}} |k\rangle \langle k+2j+1| e^{-(2j+1)i\omega_d t} \right. \\ & \left. + \sum_{k=0}^{N_{\text{max}}-1} \lambda_{k,k+1} |k\rangle \langle k+1| e^{-i\omega_d t} + \text{h.c.} \right], \quad (\text{A6}) \end{aligned}$$

where $\Delta_k = \omega_k - k\omega_d$ is the detuning between the k -th level with the k -th driving frequency harmonic. In this frame, all coupling terms, except for $|k\rangle \leftrightarrow |k+1\rangle$, and all the counter-rotating components oscillate rapidly. Therefore, we can neglect those small contributions, leading to the Hamiltonian in Eq. (1).

Appendix B: Fidelity Expressions

In this appendix, we define what are the relevant metric to benchmark the performance of our single-qubit gate. In the case of dynamics without dissipative effects, the gate infidelity is defined as $\mathcal{E}(\hat{\mathcal{U}}_Q) = 1 - \mathcal{F}[\hat{\mathcal{U}}_Q]$ where $\mathcal{F}[\hat{\mathcal{U}}_Q]$ is the gate fidelity defined as

$$\mathcal{F}[\hat{\mathcal{U}}_Q] = \frac{\text{Tr}[\hat{\mathcal{U}}_Q \hat{\mathcal{U}}_Q^\dagger]}{d(d+1)} + \frac{\left| \text{Tr}[\hat{\mathcal{U}}_Q \hat{\mathcal{U}}_I^\dagger] \right|^2}{d(d+1)}, \quad (\text{B1})$$

where $\hat{\mathcal{U}}_Q$ is the time evolution operator at the final time projected in the computational subspace and $\hat{\mathcal{U}}_I = \hat{\sigma}_{0,1}^x$ is the target π -rotation.

In presence of dissipative effects, the metric must change because the master equation strongly depends on the initial state of the system, requiring sampling to compute the gate error. Nevertheless, it is possible avoid sampling by solving the master equation for different initial states given by the poles of the Bloch sphere spanned by the eigenstates of the Pauli matrices projected in the qubit subspace $\{\hat{\sigma}_{0,1}^x, \hat{\sigma}_{0,1}^y, \hat{\sigma}_{0,1}^z\}$

$$\mathcal{F}_d[\hat{\mathcal{U}}_Q] = \frac{1}{6} \sum_{j=\pm, \pm x, \pm y} \text{Tr}[\hat{\mathcal{U}}_Q \rho_j \hat{\mathcal{U}}_Q^\dagger \mathcal{M}(\rho_j)], \quad (\text{B2})$$

where ρ_j are the eigenstates of the Pauli matrices projected in the qubit subspace $\{\sigma_{0,1}^x, \sigma_{0,1}^y, \sigma_{0,1}^z\}$, moreover, $\mathcal{M}(\rho_j)$ is the state obtained by solving Eq. (39) considering ρ_j as its initial state.

Appendix C: Third order Hamiltonian and corrections

Expanding $\hat{\mathcal{H}}_1(t)$ on Eq. (4) up to third order in Ω_x/Δ_2 and keeping only the qubit subspace and its transitions we obtain:

$$\begin{aligned}
\hat{\mathcal{H}}'_1(t) \approx & \left[\frac{\Omega_x}{2} + \frac{(4 - \lambda_2^2)\Omega_x^3}{16\Delta_2^2} \right] \hat{\sigma}_{0,1}^x + \frac{6\lambda_2\Omega_x}{48\Delta_2^5\Delta_3^2} \left[\Delta_3^2(\Delta_2^2 + (\Delta_3 - 2\Delta_2)^2\lambda_3^2)\Omega_1\dot{\Omega}_1 - (\Delta_3 - 2\Delta_2)^2(\Delta_3^2 - \Delta_2^2)\lambda_3^2\Omega_2\dot{\Omega}_2 \right] \hat{\sigma}_{1,2}^y \\
& + \frac{\lambda_2\Omega_x}{48\Delta_2^5\Delta_3^2} \left[3\Delta_3^2(\Delta_2^3 + \Delta_3(\Delta_3 - 2\Delta_2)^2\lambda_3^2)\Omega_1^2 - 3\Delta_3(\Delta_3 - 2\Delta_2)^2(\Delta_3^2 - \Delta_2^2)\lambda_3^2\Omega_2^2 + \right. \\
& \left. + \Delta_2^2\Delta_3^2(\Delta_2(31 - 14\lambda_2^2 + 10\lambda_3^2) - 3\Delta_3\lambda_3^2)\Omega_x^2 \right] \hat{\sigma}_{1,2}^x + \frac{\lambda_1\lambda_2\Omega_x}{\Delta_2^4} \left[\frac{(\Delta_2^2 - \Delta_3^2)(\Delta_3 - 2\Delta_2)}{16\Delta_3} \Omega_2^2 + \right. \\
& \left. + \frac{\Delta_2(3\Delta_2 - \Delta_3)\Omega_x^2}{48} - \frac{3(\Delta_3 - 2\Delta_2)\Omega_1(\Omega_1(\Delta_2 + \Delta_3))}{48} \right] \hat{\sigma}_{0,3}^x - \frac{\lambda_1\lambda_2\Omega_x}{\Delta_2^4} \left[\frac{3(\Delta_3 - 2\Delta_2)\Omega_1 4i\dot{\Omega}_1}{48} \right] \hat{\sigma}_{0,3}^y,
\end{aligned} \tag{C1}$$

To correct higher order terms in $\sigma_{0,1}^x$ we use the linear shift

in Eq. 18. To correct the higher order terms in $\sigma_{1,2}^x$ and $\sigma_{1,2}^y$ we follow the transformation generated by Eq. 19 introducing an auxiliary variable A defined as:

$$\begin{aligned}
A = & \frac{1}{24\Delta_2^4} \left[-\frac{(\Delta_2^2 - \Delta_3^2)(\Delta_3 - 2\Delta_2)^2}{\Delta_3^2} \lambda_3^2 \dot{F} + 3\Delta_2(\Delta_2^3 + \Delta_3(\Delta_3 - 2\Delta_2)^2\lambda_3^2)\Omega_1^2\Omega_x \right. \\
& \left. + \frac{(\Delta_2^2 - \Delta_3^2)(\Delta_3 - 2\Delta_2)^2}{\Delta_3} 3\Delta_2\lambda_3^2\Omega_2^2\Omega_x + \Delta_2^3(-3\Delta_3\lambda_3^2 + \Delta_2(31 - 14\lambda_2^2 + 10\lambda_3^2))\Omega_x^3 \right], \tag{C2}
\end{aligned}$$

with $F = \dot{\Omega}_2\Omega_2\Omega_x + (\Delta_1^2 + (\Delta_3 - 2\Delta_2)^2\lambda_3^2)\Delta_2^2\dot{\Omega}_1\Omega_1\Omega_x/(\Delta_2^2 - \Delta_3^2)(\Delta_3 - 2\Delta_2)^2\lambda_3^2$ as another auxiliary variable.

Appendix D: Magnus Expansion of Toggling Frame

To obtain β and δ_c we have to compute the computational subspace of $\hat{\mathcal{Z}}$:

$$\hat{\mathcal{Z}}_1[1,1] - \hat{\mathcal{Z}}_1[0,0] = i \int_0^T \frac{(4\Delta_2\delta_c + (4\alpha - \lambda_2^2)\Omega_x^2)\cos\theta}{4\Delta_2} + \frac{\dot{\Omega}_x(\alpha - 1)\alpha\lambda_2^2\Omega_x\sin\theta}{8\Delta_2^3} dt \tag{D1}$$

$$\hat{\mathcal{Z}}_1[0,1] = \int_0^T \frac{\Omega_x - \theta}{2} + i \frac{(4\Delta_2\delta_c + (4\alpha - \lambda_2^2)\Omega_x^2)\sin\theta}{8\Delta_2} - \frac{\Omega_x(\Delta_2 8\alpha\delta_c + (4\alpha^2 + \lambda_2^2(1 - 2\alpha)\Omega_x^2))}{16\Delta_2^2} + i \frac{\dot{\Omega}_x(\alpha - 1)\alpha\lambda_2^2\Omega_x\cos\theta}{16\Delta_2^3} dt \tag{D2}$$

Note that both Ω_x and θ are time-dependent functions in the above equations.

In order to compute the analytical DRAG prefactor, we

need the elements of the Magnus expansion of the Toggling frame of transitions $|1\rangle \rightleftharpoons |2\rangle$ and $|0\rangle \rightleftharpoons |2\rangle$. To the second order, these are:

$$\hat{\mathcal{Z}}_1[1,2] = \int_0^T \frac{\lambda_2 e^{-i\phi_1}}{4\Delta_2} \left(i(\Omega_x^2 \sin \frac{\theta}{2} - 2\dot{\Omega}_x \cos \frac{\theta}{2}) - \alpha \frac{-4i\Delta_2\dot{\Omega}_x \cos \frac{\theta}{2} + \Omega_x(2\dot{\Omega}_x + i\Delta_2\Omega_x) \sin \frac{\theta}{2}}{2\Delta_2} + \alpha^2 \frac{\Omega_x\dot{\Omega}_x \sin \frac{\theta}{2}}{\Delta_2} \right) dt \tag{D3}$$

and

$$\hat{\mathcal{Z}}_1[0,2] = \int_0^T \frac{\lambda_2 e^{-i\phi_1}}{4\Delta_2} \left((\Omega_x^2 \cos \frac{\theta}{2} + 2\dot{\Omega}_x \sin \frac{\theta}{2}) - \alpha \frac{4\Delta_2\dot{\Omega}_x \sin \frac{\theta}{2} + \Omega_x(-2i\dot{\Omega}_x + \Delta_2\Omega_x) \cos \frac{\theta}{2}}{2\Delta_2} - i\alpha^2 \frac{\Omega_x\dot{\Omega}_x \cos \frac{\theta}{2}}{\Delta_2} \right) dt \tag{D4}$$

with $\hat{\mathcal{Z}}_1[2,1] = \bar{\hat{\mathcal{Z}}}_1[1,2]$ and $\hat{\mathcal{Z}}_1[2,0] = \bar{\hat{\mathcal{Z}}}_1[0,2]$.

Appendix E: R1D Optimization

We can also optimize R1D pulses by using Eq. 35 and starting with $\Omega_1 = \sin^3 \pi t/T$. As can be seen in Fig. 8 although

we see an improvement over optimized linear DRAG, R1D does not match R2D. Plotting population evolution for a gate time of $T=7$ [ns] in Fig. 9 explains why - we see that leakage to $|3\rangle$ clearly limits our gate performance. This lends even more strength to the need for R2D pulses.

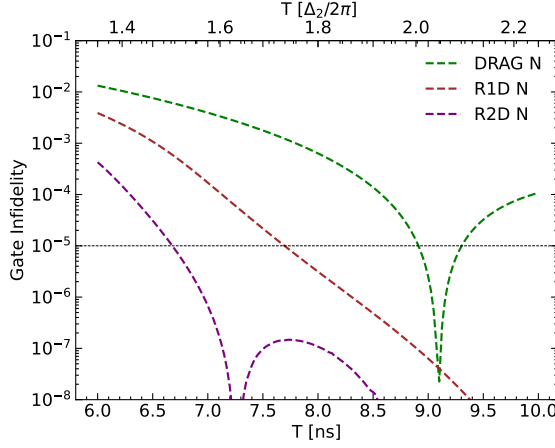


FIG. 8. Gate Infidelities for calibrated linear DRAG pulses (green), calibrated R1D pulses (brown) and calibrated R2D pulses (purple). Although R1D performs better than linear DRAG, it fails to achieve infidelities above 99.999 % for gate times shorter than $T \approx 7.7$ ns

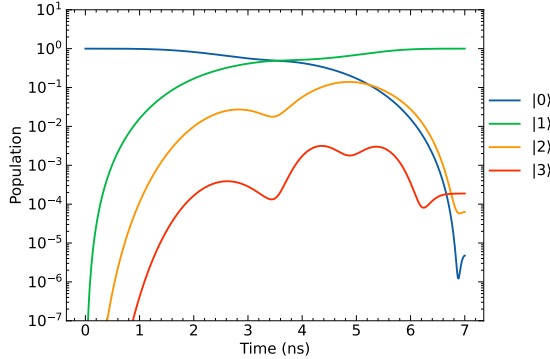


FIG. 9. Evolution of population for a π gate using a calibrated R1D pulse. As can be seen, leakage to $|3\rangle$ is substantial and hampers gate performance

Appendix F: Ansatz Selection

Here, we will show how to obtain the pulse from Eq. (17). Our starting point is the boundary conditions given in Eq (6b) together with the additional one provided by both R1D and R2D, thus, we can choose a Fourier ansatz of the form

$$\Omega(t) = \frac{1}{2} + \frac{1}{2(k-1)} \left[\cos \left[j \frac{2\pi}{T} t \right] - k \cos \left[n \frac{2\pi}{T} t \right] \right], \quad (\text{F1})$$

this functional form ensures that the first and third derivatives are zero at $t = 0$ and $t = T$, then, we need to find the condition for the second derivative at both times, obtaining that the pulse from Eq. (17) achieves the lower error for a gate faster than ten nanoseconds.

$$\ddot{\Omega} = - \left[\frac{2\pi}{T} \right]^2 \left[j^2 \cos \left[j \frac{2\pi}{T} t \right] - kn^2 \cos \left[n \frac{2\pi}{T} t \right] \right]. \quad (\text{F2})$$

To obtain null derivative at $t = 0$ and $t = T$, we obtain the relation

$$k = \frac{j^2}{n^2}, \quad \forall k \neq 1. \quad (\text{F3})$$

Table I shows the optimal gate time T to obtain gate error below 10^{-4} for different value of the triad $\{n, j, k\}$. Obtaining that

n	j	k	$T_{99.99}$ (ns)
1	2	4	10.43
1	3	9	8.42
1	4	16	8.45
1	5	25	8.60
2	3	9/4	18.0
2	4	8	18.0
2	5	25/4	18.0

TABLE I. Optimal gate times T achieving an error below 10^{-4} for different choices of the ansatz parameters $\{n, j, k\}$. The highlighted entry corresponds to the fastest configuration.

[1] P. Krantz, M. Kjaergaard, F. Yan, T. P. Orlando, S. Gustavsson, and W. D. Oliver, *A quantum engineer's guide to superconducting qubits*, *Applied Physics Reviews* **6**, 021318 (2019).

[2] A. Blais, A. L. Grimsmo, S. M. Girvin, and A. Wallraff, *Circuit Quantum Electrodynamics*, *Reviews of Modern Physics* **93**, 025005 (2021), arXiv:2005.12667 [quant-ph].

[3] J. Koch, T. M. Yu, J. Gambetta, A. A. Houck, D. I. Schuster, J. Majer, A. Blais, M. H. Devoret, S. M. Girvin, and R. J. Schoelkopf, *Charge-insensitive qubit design derived from the cooper pair box*, *Phys. Rev. A* **76**, 042319 (2007).

[4] Z. Chen, J. Kelly, C. Quintana, R. Barends, B. Campbell, Y. Chen, B. Chiaro, A. Dunsworth, A. G. Fowler, E. Lucero,

et al., *Measuring and suppressing quantum state leakage in a superconducting qubit*, *Phys. Rev. Lett.* **116**, 020501 (2016).

[5] F. Motzoi, J. M. Gambetta, P. Rebentrost, and F. K. Wilhelm, *Simple pulses for elimination of leakage in weakly nonlinear qubits*, *Phys. Rev. Lett.* **103**, 110501 (2009).

[6] F. Motzoi and F. K. Wilhelm, *Improving frequency selection of driven pulses using derivative-based transition suppression*, *Phys. Rev. A* **88**, 062318 (2013).

[7] L. S. Theis, F. Motzoi, S. Machnes, and F. K. Wilhelm, *Counteracting systems of diabaticities using DRAG controls: The status after 10 years*, *EPL (Europhysics Letters)* **123**, 60001 (2018).

[8] J. M. Gambetta, F. Motzoi, S. T. Merkel, and F. K. Wilhelm, *Analytic control methods for high-fidelity unitary operations in a weakly nonlinear oscillator*, *Phys. Rev. A* **83**, 012308 (2011).

[9] B. Li, T. Calarco, and F. Motzoi, *Experimental error suppression in Cross-Resonance gates via multi-derivative pulse shaping*, *npj Quantum Information* **10**, 1–10 (2024).

[10] B. Li, F. Cárdenas-López, A. Lupascu, and F. Motzoi, *Universal pulses for superconducting qudit ladder gates*, *PRX Quantum* **6**, 030357 (2025).

[11] E. Hyypä, A. Vepsäläinen, M. Papič, C. F. Chan, S. Inel, A. Landra, W. Liu, J. Luus, F. Marxer, C. Ockeloen-Korppi, *et al.*, *Reducing leakage of single-qubit gates for superconducting quantum processors using analytical control pulse envelopes*, *PRX Quantum* **5**, 030353 (2024).

[12] B. Chiaro and Y. Zhang, *Active leakage cancellation in single qubit gates*, *Phys. Rev. Lett.* **135**, 130601 (2025).

[13] B. Khani, J. M. Gambetta, F. Motzoi, and F. K. Wilhelm, *Optimal generation of Fock states in a weakly nonlinear oscillator*, *Physica Scripta* **2009**, 014021 (2009).

[14] B. Li, T. Calarco, and F. Motzoi, *Nonperturbative Analytical Diagonalization of Hamiltonians with Application to Circuit QED*, *PRX Quantum* **3**, 030313 (2022).

[15] J. R. Schrieffer and P. A. Wolff, *Relation between the anderson and kondo hamiltonians*, *Phys. Rev.* **149**, 491–492 (1966).

[16] L. H. Pedersen, N. M. Møller, and K. Mølmer, *Fidelity of quantum operations*, *Physics Letters A* **367**, 47–51 (2007).

[17] R. Wang, Y. Feng, Y. Zhang, J. Ding, B. Li, F. Motzoi, Y. Gao, H. Xu, Z. Yang, W. Nuerbolati, *et al.*, *Suppressing Spurious Transitions Using Spectrally Balanced Pulse*, *Physical Review Letters* **135**, 160804 (2025).

[18] F. Marxer, J. Mrožek, J. Andersson, L. Abdurakhimov, J. Adam, V. Bergholm, R. Beriwal, C. F. Chan, S. Dahl, S. R. Das, *et al.*, *Above 99.9superconducting quantum device* (2025), [arXiv:2508.16437 \[quant-ph\]](https://arxiv.org/abs/2508.16437).

[19] J. J. Burnett, A. Bengtsson, M. Scigliuzzo, D. Niegce, M. Kudra, P. Delsing, and J. Bylander, *Decoherence benchmarking of superconducting qubits*, *npj Quantum Information* **5**, 54 (2019).

[20] S. E. de Graaf, L. Faoro, L. B. Ioffe, S. Mahashabde, J. J. Burnett, T. Lindström, S. E. Kubatkin, A. V. Danilov, and A. Y. Tzalenchuk, *Two-level systems in superconducting quantum devices due to trapped quasiparticles*, *Science Advances* **6**, eabc5055 (2020), <https://www.science.org/doi/pdf/10.1126/sciadv.abc5055>.

[21] N. Wu, J. Lin, C. Xie, Z. Guo, W. Huang, L. Zhang, Y. Zhou, X. Sun, J. Zhang, W. Guo, *et al.*, *In situ mixer calibration for superconducting quantum circuits*, *Applied Physics Letters* **125**, 204003 (2024).

[22] S. Gustavsson, O. Zwier, J. Bylander, F. Yan, F. Yoshihara, Y. Nakamura, T. P. Orlando, and W. D. Oliver, *Improving quantum gate fidelities by using a qubit to measure microwave pulse distortions*, *Phys. Rev. Lett.* **110**, 040502 (2013).

[23] L.-L. Guo, P. Duan, S. Zhang, X.-X. Yang, C. Zhang, L. Du, H.-F. Zhang, H.-R. Tao, T.-L. Wang, Z.-L. Jia, *et al.*, *Universal scalable characterization and correction of pulse distortions in controlled quantum systems*, *Phys. Rev. Appl.* **21**, 064060 (2024).

[24] W. S. Warren, *Effects of arbitrary laser or nmr pulse shapes on population inversion and coherence*, *The Journal of Chemical Physics* **81**, 5437–5448 (1984).

[25] U. Haeberlen, *High Resolution NMR in Solids: Selective Averaging*, *Advances in Magnetic Resonance*, Supplement 1 (Academic Press, New York, NY, 1976).

[26] A. Brinkmann, *Introduction to average hamiltonian theory. i. basics*, *Concepts in Magnetic Resonance Part A* **45A**, e21414 (2016).

[27] S. Blanes, F. Casas, J. Oteo, and J. Ros, *The magnus expansion and some of its applications*, *Physics Reports* **470**, 151–238 (2009).

[28] S. Kirchhoff, F. K. Wilhelm, and F. Motzoi, *Correction formulas for the mølmer-sørensen gate under strong driving*, *PRX Quantum* **6**, 010328 (2025).

[29] Y. Gao, A. Galicia, J. D. D. C. Jesus, Y. Liu, Y. Haddad, D. A. Volkov, J. R. Guimarães, H. Bhardwaj, M. Jerger, M. Neis, *et al.*, *Ultrafast single qubit gates through multi-photon transition removal* (2025), [arXiv:2511.22365 \[quant-ph\]](https://arxiv.org/abs/2511.22365).

[30] D. Manzano, *A short introduction to the lindblad master equation*, *AIP Advances* **10**, 10.1063/1.5115323 (2020).

[31] IBM Quantum, Ibm quantum platform, https://quantum.cloud.ibm.com/computers?system=ibm_pittsburgh (2025), accessed: 2025-12-10.

[32] M. D. Bowdrey, D. K. Oi, A. J. Short, K. Banaszek, and J. A. Jones, *Fidelity of single qubit maps*, *Physics Letters A* **294**, 258–260 (2002).